NASA TR R-116

NATIONAL AERONAUTICS AND SPACE ADMINISTRATION

TECHNICAL REPORT
R-116

NUMERICAL PREDICTIONS OF RADIATIVE INTERCHANGE BETWEEN CONDUCTING FINS WITH MUTUAL IRRADIATIONS

By MAX. A. HEASLET and HARVARD LOMAX

1961

For sale by the Superintendent of Documents, U.S. Government Printing Office, Washington 25, D.C. Yearly subscription, $15; foreign, $19; single copy price varies according to size -------- Price 35 cents

TECHNICAL REPORT R-116

NUMERICAL PREDICTIONS OF RADIATIVE INTERCHANGE BETWEEN CONDUCTING FINS WITH MUTUAL IRRADIATIONS

By MAX. A. HEASLET and HARVARD LOMAX

Ames Research Center
Moffett Field, Calif.

TECHNICAL REPORT R-116

NUMERICAL PREDICTIONS OF RADIATIVE INTERCHANGE BETWEEN CONDUCTING FINS WITH MUTUAL IRRADIATIONS

By Max. A. Heaslet and Harvard Lomax

SUMMARY

Analytical and numerical methods are developed that predict the flux of radiant energy from a family of thin, planar, conducting fins. For a symmetrical array of fins, extending out from a common edge, conducting heat internally, and radiating diffusely, a nonlinear integro-differential equation is derived and solved. Specific results are given for parametric variations of conduction, emissivity, fin geometry, and base temperature. The techniques of calculation are studied with possible extensions in mind.

INTRODUCTION

The present paper has a dual objective. First, it will furnish predictions of the radiative interchange of heat between an assemblage of conducting, planar fins subjected to incident radiant energy in a diathermanous environment. Second, it will develop a combined analytical and numerical attack on the type of integro-differential equation associated with problems of this general character. The results represent one unit of a program of radiative heat calculations now under way at the Ames Research Center, NASA. Specific results, of use in design studies, will be given for a particular family of fin orientations. An attempt will be made, at the same time, to develop the iterative mathematical methods in such a way that extensions to problems of similar type are readily apparent. The numerical calculations were carried out on an IBM 704 installation, and the total computing time for the results to be shown required approximately one hour of machine time.

The design of space vehicles has focused attention on finned surfaces and their use as radiative disposers of waste heat or as collectors of incident solar energy. In such a case the nature of the external environment precludes the need to consider convective heat transport. A significant physical idealization, and the one to be considered here, arises when one represents the fins as a symmetrical array of planar surfaces of thin plates of thickness $2t$, and with a common edge, see figure 1. The length of the common edge is sufficiently large in comparison with the length L of the plates normal to this edge that the heat exchange can be studied in the two-dimensional cross-plane, figure 1(b). The number of fins n is an arbitrary integer >1 and the included angle $\theta=360°/n$. The plates are alike in physical structure with a known coefficient of conductivity, the radiative emission is diffuse, and a gray-body type of analysis is employed; that is, no dependence on radiation wave length is included. The symmetry of the configuration is retained and subcases of practical interest appear if it is assumed at the outset that a fixed temperature T_b is imposed along the common axis ($x=0$, $y=0$) and a uniform distribution of incident diffuse radiation is assumed to be directed into the open face of each of the angular sectors. A brief derivation of the governing equations will be given in the following section.

In a recent paper, Sparrow, Gregg, Szel, and Manos, reference 1, have solved a special form of this problem. Specifically, they omit heat conduction within the plates themselves and consider no external source field. In effect, they study the case of infinite thermal conductivity and determine the radiant interchange of energy between the two plates of figure 1(b) when surface temperature is a constant. The integral equation

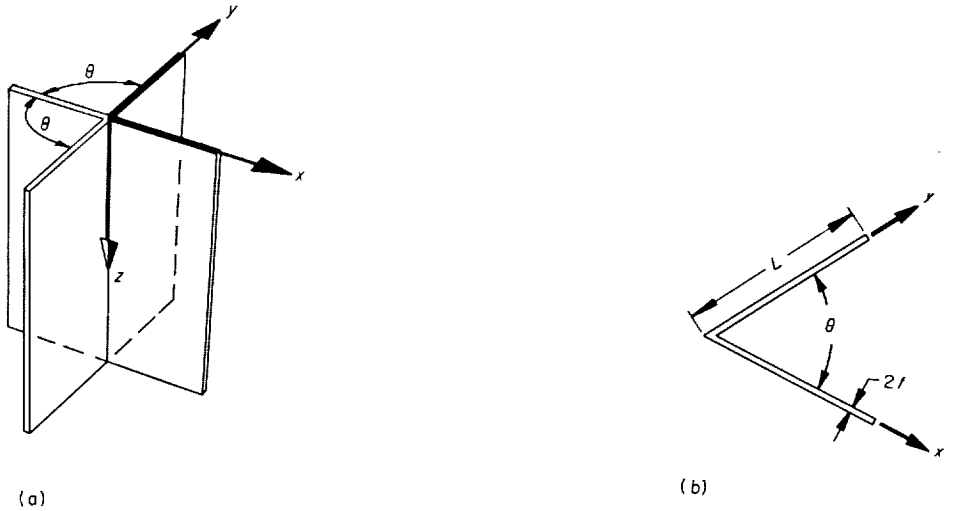

(a) Three-dimensional idealization.

(b) Two-dimensional section.

FIGURE 1.—Arrangements of fins.

that characterizes the transferal of energy was replaced in their analyses by a finite difference scheme that led, in turn, to the study of simultaneous, linear, algebraic equations. To achieve a reasonable degree of accuracy in the final solution it was necessary to use a rather large number of simultaneous equations. Even then, some sacrifice in accuracy was incurred in the immediate neighborhood of the common edge (a singular point in the kernel of the integral equation). We shall here approach the general problem from a different point of view and use an iterative process that comprises a wedding of machine calculation and the Liouville-Neumann method of solving a Fredholm integral equation of the second kind. The analysis of reference 1 is a linear one; when conduction and variation in plate temperatures are considered, nonlinearities appear and the analysis involves the solution of an integro-differential equation, but no unsurmountable difficulties beset the iterative method of attack, and adequate convergence of the numerical process is retained.

In another paper, Eckert, Irvine, and Sparrow, reference 2, have derived the defining equations under more general conditions involving thermal conductivity within the fins and differing fin geometry. Readers interested in extensions of the theory to other configurations should refer to that work. The restriction to thin planar fins was proposed in reference 2 as a reasonable simplification that produces results of general interest and at the same time lessens the number of parameters affecting the predictions. The techniques of calculation presented here can be extended, however, to apply to additional cases.

The analytical section which follows reviews, at the outset, the derivation of the integral and differential equations controlling the heat exchange. We next show how some information regarding the solution can be achieved analytically. The bulk of the contribution is, however, contained in the iterative numerical calculations carried out on an electronic computer. The final results are graphical representations of temperature distribution along the fins, the thermal current flow within the fins, and the local net heat-transfer function for a range of physical parameters including the angle θ, the emissivity or reflectivity of the plates, and thermal conductivity. The nomenclature follows generally that used in the references mentioned above, but some differences do appear. The Table of Symbols defines all important variables.

Readers with special interest in the physical predictions may wish to confine their attention to the basic assumptions, the defining equations, and the subsequent presentation of results. A final section has been added, however, in which the adaptation of the problem to digital computing machines is discussed in some detail. This latter section is intended to aid people con-

cerned with similar predictions. Finally, a more general discussion of improvements in the convergence of numerical iterations is included.

TABLE OF IMPORTANT SYMBOLS

a	$\cos\theta$
$B(x)$, $B(y)$	combined radiative flux (emitted plus reflected) from x or y (cal/cm² sec)
$B^*(\xi)$, $B^*(\eta)$	dimensionless combined flux, $\frac{B}{\sigma T_b^4}$
$B_I^*(\xi)$	radiation function defined in equation (20)
e	uniform incident radiation flux from external source (cal/cm² sec)
$G(\xi)$	function introduced in equation (18b)
$H(x)$	incident radiant flux at x (cal/cm² sec)
k	thermal conductivity
$K(\xi, \eta)$	kernel function introduced in equation (9a)
L	fin length
N_e	dimensionless flux, $\frac{e}{\sigma T_b^4}$
N_c	conduction parameter $\frac{\sigma L^2 T_b^3}{kt}$
$q(x)$	local thermal current inside fin (cal/sec)
$q^*(\xi)$	see equation (11)
$Q(x)$	local heat flux (cal/cm² sec)
$Q^*(\xi)$	see equation (12)
$\mathcal{Q}(x)$	integrated heat flux (cal/cm sec)
$\mathcal{Q}^*(\xi)$	see equation (13)
r	distance between two points
S_x, S_y	areas on two fins
t	half-thickness of fin
$T(x)$	absolute temperature, local
T_b	temperature at x y 0
$T^*(\xi)$	dimensionless temperature $\frac{T}{T_b}$
x, y	nonorthogonal coordinates along fins
z	coordinate along common axis of fins
α	gray-body absorptivity, 1 - ρ
ϵ	gray-body emissivity
ξ, η	dimensionless coordinates $\frac{x}{L}, \frac{y}{L}$
θ	angle between adjacent plates
ρ	gray-body reflectivity, $1-\alpha$

ANALYSIS

GOVERNING EQUATIONS

Figure 2 shows the idealization of the assumed geometry. The symmetry of the assumptions permits one to consider only two plates of thickness $2t$, of length L and infinite extent normal to the plane of the paper, and forming the angle θ at their common edge. The nonorthogonal coordinate axes x and y extend along the direction of the plates and for small values of t/L may be assumed either to coincide with the plate surfaces or to lie along the center lines. Let dS_x and dS_y be representative area differentials on each surface, and denote by $B(x)$ the combined radiation flux (energy per unit time and area) at the point x.

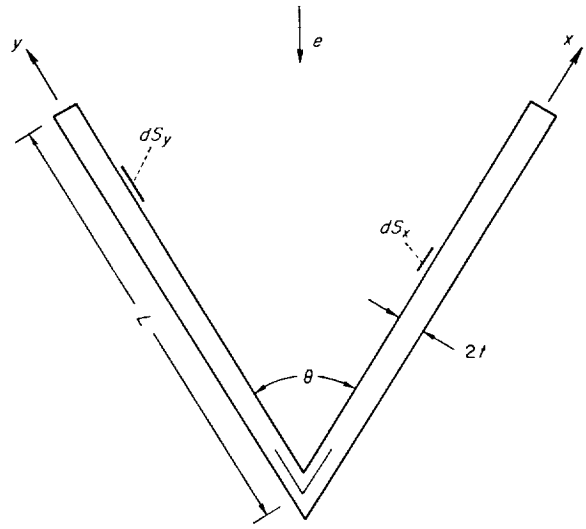

FIGURE 2.—Fin pair with incident radiation.

Thus, $B(x)$ embraces both emitted and reflected energy, and the emission is adapted from the Stefan-Boltzmann law in the form $\epsilon\sigma T^4$, where ϵ is surface gray-body emissivity and σ is the Stefan-Boltzmann constant. Incident energy per unit time and area at x is denoted by $H(x)$ so that reflected energy flux is $\rho H(x) \equiv (1-\alpha)H(x)$, where α is absorptivity. Combined flux then becomes

$$B(x) = \epsilon\sigma T(x)^4 + (1-\alpha)H(x) \tag{1}$$

From an external source we assume a diffuse flow of energy through the area connecting the fin tips. The magnitude of the flux is e.

The incident energy flux at x is composed of two parts: first, the flux arriving from all posi-

tions y on the opposing plate; second, the flux from the external source. Combining these two effects, one has

$$H(x)=\int_{S_y} B(y)dF_{x-y}+eF_{x-S_e} \tag{2}$$

where dF_{x-y} is the angle factor under which dS_y is seen from x, and F_{x-S_e} is the angle factor under which the surface S_e between the fin tips is seen from x.

In a two-dimensional configuration the angle factor of an infinitesimal area of unit width, $dS_2=(1)(ds_2)$, as viewed from a point P_1, is

$$dF_{1-2}=\frac{1}{2}\frac{d}{ds_2}\left(\frac{\Delta}{r}\right)ds_2 \tag{3}$$

where, as in figure 3, r is the distance P_1P_2 and

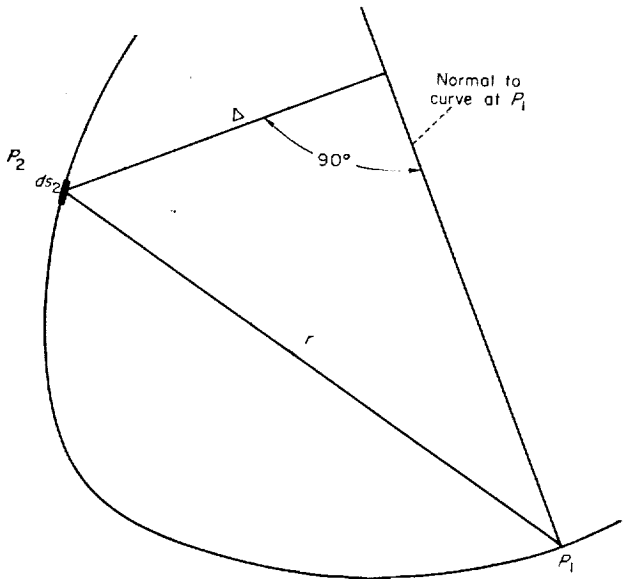

FIGURE 3.—Sketch showing variables in two-dimensional angle factor.

Δ is the length of a perpendicular dropped from P_2 to the surface normal at P_1. Thus

$$dF_{x-y}=\frac{1}{2}\frac{d}{dy}\frac{y\cos\theta-x}{(x^2+y^2-2xy\cos\theta)^{1/2}}dy$$

$$=\frac{(1-a^2)}{2}\frac{xydy}{(x^2+y^2-2axy)^{3/2}} \tag{4}$$

where $a=\cos\theta$. For flux at x produced by the uniform incident energy, similar considerations give

$$eF_{x-S_e}=\frac{e}{2}\left[1-\frac{La-x}{(L^2+x^2-2aLx)^{1/2}}\right] \tag{5}$$

Equations (1), (2), (4), and (5) yield the integral equation for $B(x)$:

$$B(x)=\epsilon\sigma T(x)^4+\frac{(1-\alpha)(1-a^2)}{2}\int_0^L B(y)\frac{xydy}{(x^2+y^2-2axy)^{3/2}}+\frac{e(1-\alpha)}{2}\left[1-\frac{La-x}{(L^2+x^2-2aLx)^{1/2}}\right] \tag{6}$$

The differential equation governing the conduction within the fin balances the energy transport, as given by Fourier's law, and the radiation flux from the exterior surfaces. Applying this equality to a two-dimensional strip of unit width, one gets

$$\frac{d}{dx}\left(kt\frac{dT}{dx}\right)=B(x)-H(x) \tag{7}$$

In addition to equations (6) and (7), the following boundary conditions are specified

$$\left.\begin{aligned} T&=T_b && \text{at } x=0\\ -k\left(\frac{dT}{dx}\right)&=B(L)-H(L) && \text{at } x=L\end{aligned}\right\} \tag{8}$$

It is convenient to rewrite the governing equations as they appear in a normalized system of variables (see Table of Symbols). One then gets

$$B^*(\xi)=\epsilon T^*(\xi)^4+\frac{(1-\alpha)N_c}{2}\left[1-\frac{a-\xi}{(1+\xi^2-2a\xi)^{1/2}}\right]+\frac{(1-\alpha)(1-a^2)}{2}\int_0^1 B^*(\eta)K(\xi,\eta)d\eta \tag{9a}$$

where

$$K(\xi,\eta)=\frac{\xi\eta}{(\xi^2+\eta^2-2a\xi\eta)^{3/2}}$$

$$\frac{d^2T^*}{d\xi^2}=\frac{N_c}{(1-\alpha)}\left[\epsilon T^*(\xi)^4-\alpha B^*(\xi)\right] \tag{9b}$$

with boundary conditions

$$\left.\begin{aligned} T^*(0)&=1\\ \frac{dT^*(1)}{d\xi}&=-\frac{N_ct}{L}\left[B^*(1)-H^*(1)\right]\\ &\approx-\frac{N_ct}{L}\left[\epsilon T^*(1)^4-\alpha N_c\right]\end{aligned}\right\} \tag{9c}$$

The following relations also apply

$$B^*(\xi)-H^*(\xi)=\epsilon T^*(\xi)^4-\alpha H^*(\xi)$$
$$=\frac{\epsilon T^*(\xi)^4-\alpha B^*(\xi)}{1-\alpha} \quad (9d)$$

TRANSFER FUNCTIONS

A straightforward solution of equations (9) involves the determination of the two functions $B^*(\xi)$ and $T^*(\xi)$ by solving the integral equation (9a) and the differential equation (9b). From this analysis, which is obviously a nonlinear one, follow predictions of local temperature, local current flow within the fins, local heat flux from the surfaces, and total heat flux. The results to be given later will be expressed in terms of starred values defined by the following relation:

Temperature, °K

$$\left.\begin{aligned}&\text{Physical variation:}\quad T=T(x)\\&\text{Predicted variation:}\quad T^*(\xi)=\frac{T(Lx/L)}{T_b}\end{aligned}\right\} \quad (10)$$

Local thermal current inside fin (cal/sec)

$$\left.\begin{aligned}&\text{Physical variation:}\quad q(x)=-\frac{2kt\,dT(x)}{dx}\\&\text{Predicted variation:}\quad \frac{q^*(\xi)}{2L}=\frac{q(Lx/L)}{\sigma T_b^4 2L}=-\frac{dT^*(\xi)/d\xi}{N_c}\end{aligned}\right\} \quad (11)$$

Local heat flux (cal/cm² sec)

$$\left.\begin{aligned}&\text{Physical variation:}\quad Q(x)=B(x)-H(x)=\epsilon\sigma T(x)^4-\alpha H(x)\\&\text{Predicted variation:}\quad Q^*(\xi)=\frac{Q(Lx/L)}{\sigma T_b^4}=\frac{d^2T^*(\xi)/d\xi^2}{N_c}\end{aligned}\right\} \quad (12)$$

Integrated heat flux (cal/cm sec)

$$\left.\begin{aligned}&\text{Physical variation:}\quad \mathcal{Q}=\int_0^L Q(x)dx\\&\text{Predicted variation:}\quad \frac{\mathcal{Q}^*}{L}=\int_0^L\frac{Q[L(x/L)]dx}{L\sigma T_b^4}=\frac{1}{N_c}\left[\frac{dT^*(1)}{d\xi}-\frac{dT^*(0)}{d\xi}\right]\end{aligned}\right\} \quad (13)$$

ANALYTIC PROCEDURES

A new independent variable $u(\xi)$ where

$$u(\xi)=\frac{1}{N_c}\frac{dT^*(\xi)}{d\xi} \quad (14)$$

is next to be introduced in equations (9). The analysis is thus cast in a form where the unknown is a constant factor times the local thermal current. From the first boundary condition of equation (9c)

$$T^*(\xi)=1+N_c\int_0^\xi u(\xi_1)d\xi_1 \quad (15)$$

Equation (9b) then becomes

$$\frac{\alpha}{1-\alpha}B^*(\xi)=-\frac{du(\xi)}{d\xi}+\frac{\epsilon T^*(\xi)^4}{1-\alpha} \quad (16)$$

from which equation (9a) can be rewritten as an integro-differential equation

$$\frac{du(\xi)}{d\xi}=\epsilon\left\{\left[1+N_c\int_0^\xi u(\xi_1)d\xi_1\right]^4-\frac{\alpha}{\epsilon}N_c\right\}$$
$$+\frac{(1-\alpha)(1-a^2)}{2}\int_0^1\left(\frac{du}{d\eta}-\frac{\epsilon}{1-\alpha}\left\{\left[1+N_c\right.\right.\right.$$
$$\left.\left.\left.\int_0^\eta u(\xi_1)d\xi_1\right]^4-\frac{\alpha}{\epsilon}N_c\right\}\right)K(\xi,\eta)d\eta \quad (17a)$$

with the boundary condition

$$u(1)\approx-\frac{t}{L}\epsilon\left\{\left[1+N_c\int_0^1 u(\xi_1)d\xi_1\right]^4-\frac{\alpha}{\epsilon}N\right\} \quad (17b)$$

For purposes of discussion, it is also convenient to rewrite equation (17a) in the alternative form

$$\frac{du(\xi)}{d\xi}=\left[G(\xi)-\frac{(1-a^2)}{2}\int_0^1 G(\eta)K(\xi,\eta)d\eta\right]$$
$$+\frac{(1-\alpha)(1-a^2)}{2}\int_0^1\frac{du(\eta)}{d\eta}K(\xi,\eta)d\eta \quad (18a)$$

where

$$G(\xi)=\epsilon\left\{\left[1+N_c\int_0^{\xi}u(\xi_1)d\xi_1\right]^4-\frac{\alpha}{\epsilon}N_c\right\} \quad (18b)$$

Before proceeding to a discussion of general cases, two immediate simplifications should be noted in the governing equations. The first of these occurs when no fixed value of T_b is imposed and the entire configuration is allowed to seek the equilibrium state consistent with the incoming radiation from the external source; the second occurs when conductivity k becomes very large and the parameter N_c consequently approaches zero. These special cases will be treated next.

In this case, total equilibrium can be achieved by imposing local equilibrium conditions. Thus, we set

$$B^*(\xi)-H^*(\xi)-\epsilon T^*(\xi)^4-\alpha H^*(\xi)=0$$

and under these conditions $T^*(\xi)=1$ where the reference temperature T_b is yet to be determined. If one then returns directly to equation (6), the resulting equation is

$$B^*(\xi)=\frac{N_c}{2}\left[1-\frac{a-\xi}{(1+\xi^2-2a\xi)^{1/2}}\right]+\frac{(1-a^2)}{2}\int_0^1 B^*(\eta)K(\xi,\eta)d\eta$$

and the solution is $B^*(\xi)=H^*(\xi)=N_c=\text{const}$. Equilibrium conditions thus yield

$$\alpha e=\sigma\epsilon T^4$$

and the uniform equilibrium temperature is

$$T_E=\left(\frac{e}{\sigma}\right)^{1/4}\left(\frac{\alpha}{\epsilon}\right)^{1/4} \quad (19)$$

Consider next the infinite conduction case, $N_c=0$. Again, from equations (9b) and (9c), $T^*(\xi)=1$ where T_b has an assigned value different from the particular equilibrium value of equation (19). From either equation (17) or (9a) it can be shown that the transformation

$$B_I^*(\xi)=\frac{B^*(\xi)-N_c}{\epsilon-\alpha N_c} \quad (20)$$

reduces the integral equation to the form

$$B_I^*(\xi)=1+\frac{(1-\alpha)(1-a^2)}{2}\int_0^1 B_I^*(\eta)K(\xi,\eta)d\eta \quad (21)$$

Equation (21) implies that under proper normalization of the dependent variable the case of infinite conductivity and uniform incident radiation can be reduced to a study of radiative transfer for which no external source appears, conduction is disregarded, and the temperature of the fin is held fixed. The problem then reverts to the type studied in the paper of Sparrow and collaborators. Solutions of equation (21), for an extensive range of the parameters α and $a=\cos\theta$, will be given later.

The integro-differential equation (18a) as well as equations (9a) and (21) are directly associated with the classical Fredholm integral equation of the second kind

$$g(\xi)=f(\xi)+\lambda\int_0^1 g(\eta)K(\xi,\eta)d\eta \quad (22)$$

where $0\leq\lambda=(1-\alpha)\ (1-a^2)/2\leq 1/2$. One might reasonably expect, therefore, success in achieving a series expansion in powers of λ, the so-called Liouville-Neumann expansion of the solution. This idea controls the work to be developed later. It is also important to note the nature of the kernel function $K(\xi,\eta)$. Figure 4 shows a sketch

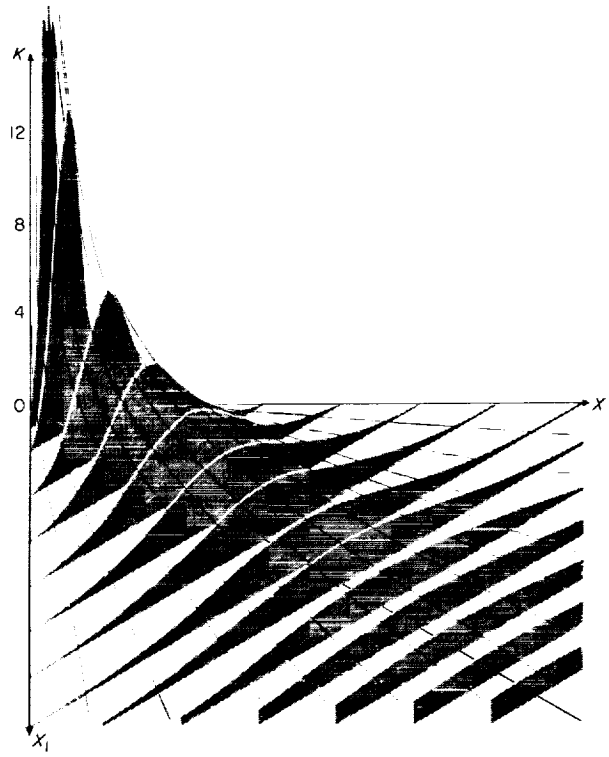

FIGURE 4.—Kernel function in radiation integral equation.

of $K(\xi, \eta)$. The function is symmetric, is never negative, and varies inversely with distance from the origin along all rays through the origin except in the coordinate planes $\xi=0$ and $\eta=0$. The function is not bounded throughout the entire region of integration but, rather, increases indefinitely as one approaches the origin along an arbitrary line $\xi/\eta = \text{const}$. This means that some care must be exercised in using theorems drawn from the theory of integral equations. In this particular case, however, the kernel is integrable and no special difficulty is encountered in extending the analysis. The integral of the kernel is, in fact, a monotonic decreasing function in the variable ξ

$$0\leq\int_0^1 K(\xi,\eta)d\eta=\frac{1}{1-a^2}\left[1+\frac{a-\xi}{(1+\xi^2-2a\xi)^{1/2}}\right]\leq\frac{1}{1-a} \tag{23}$$

The geometry of the problem indicates intuitively that some simplification should be possible in estimating conditions at the inner corner of the plates since the extent of the fins becomes effectively infinite. A more precise development of this observation proceeds as follows. In equation (22) set $\xi/\eta = \tau$. One then gets

$$g(\xi)=f(\xi)+\lambda\int_\xi^\infty \frac{g(\xi/\tau)d\tau}{(1+\tau^2-2a\tau)^{3/2}}$$

Passing to the limit as $\xi \to 0$, one has

$$g(0)=f(0)+\lambda\int_0^\infty \frac{g(0)d\tau}{(1+\tau^2-2a\tau)^{3/2}}$$

$$=f(0)+\frac{\lambda g(0)}{1-a}$$

and, therefore

$$g(0)=\frac{f(0)}{1-\lambda/(1-a)}$$

$$=\frac{f(0)}{1-(1-\alpha)(1+a)/2} \tag{24}$$

This fix on the corner value of the unknown is of considerable value in numerical calculations since, in spite of the fact that the magnitude of $g(0)$ is readily determined, a singularity in $dg/d\xi$ exists at the corner and affects any techniques based on finite difference methods.

In application to the general equation (18a), it follows that the corner value of $du/d\xi$ is

$$\frac{du(0)}{d\xi}=\frac{(\epsilon-\alpha N_e)(1-a)}{1+\alpha-a(1-\alpha)} \tag{25}$$

since, from equation (18b), $G(0)=\epsilon-\alpha N_e$.

It is also possible to show that the power series resulting from an iterative expansion of equation (18a) must also converge. If the bracketed term on the right is denoted $F(\xi)$, the iterative expansion becomes

$$\frac{du(\xi)}{d\xi}=F(\xi)+\frac{(1-\alpha)(1-a^2)}{2}\int_0^1 F(\xi_1)K(\xi,\xi_1)d\xi_1$$

$$+\sum_{n=2}^{\infty}\left[\frac{(1-\alpha)(1-a^2)}{2}\right]^n\int_0^1 K(\xi,\xi_1)$$

$$\int_0^1 K(\xi_1,\xi_2)\ldots\int_0^1 K(\xi_{n-1},\xi_n)F(\xi_n)d\xi_1\ldots d\xi_n \tag{26}$$

The reasoning whereby the series convergence is demonstrated may be shown by considering the case in which heat energy is to be radiated away from the configuration; that is, when $T_b \geq T_E$. It is obvious then that the thermal current must flow outward along the fin and that $u(\xi) = [dT^*(\xi)/d\xi]/N_c \leq 0$. Thus

$$\epsilon\left\{\left[1+N_c\int_0^1 u(\xi_1)d\xi_1\right]^4 - \frac{\alpha}{\epsilon}N_e\right\}\leq G(\xi)\leq\epsilon\left(1-\frac{\alpha}{\epsilon}N_e\right) \tag{27}$$

and since, from equation (19),

$$\frac{\alpha N_e}{\epsilon}=\left(\frac{T_E}{T_b}\right)^4=T_E{}^{*4} \tag{28}$$

equation (27) yields

$$\epsilon[T^{*4}(1)-T_E{}^{*4}]\leq G(\xi)\leq\epsilon[T^{*4}(0)-T_E{}^{*4}] \tag{29}$$

The function of $G(\xi)$ is therefore a positive bounded function, and the magnitude of the function $F(\xi)$ in equation (26) is also less than some finite constant R since the integrated kernel is bounded. Finally, repeated use of equation (23) shows that

the infinite series must converge to an absolute value not in excess of

$$R\left\{1+\sum_{n=1}^{\infty}\left[\frac{(1-\alpha)(1+a)}{2}\right]^n\right\}=\frac{R}{2-(1-\alpha)(1+a)} \tag{30}$$

The analytical considerations have thus established the exact value of $du(0)/d\xi$ in general or, in other terms, the corner value of the surface heat flux per unit area. It has also been possible to show that when the function $F(\xi)$ of equation (26) is known explicitly, a converging iterative solution is possible. In the case of infinite conduction, where the problem becomes one of solving the integral equation (21), the numerical calculations follow precisely the steps prescribed in the series development. When finite conduction occurs, $F(\xi)$ in equation (26) is a functional of $u(\xi)$ and the numerical calculations must include an iterative evaluation of $F(\xi)$. In the final section of this paper the programming of this calculation will be discussed.

It should be remarked that a purely analytical attack on the iterative process becomes excessively complex even in the special case characterized by equation (21). The singular nature of the kernel at $\xi=\eta=0$, which is a result of the corner between adjacent fins, is the principal source of the difficulty and it appears that the general solution of equation (21) has the form

$$B_I^*(\xi)=\sum_n a_n\xi^n+\sum_r\sum_s b_{rs}\xi^r \ln^s \xi$$

The nature of this solution accounts for the singular behavior of $dB_I^*/d\xi$ at the corner. A similar expansion should apply locally for the nonlinear case with conductivity.

PRESENTATION OF RESULTS

Before presenting the numerical predictions of the general solutions, the analytic result of equation (25) will be recast in more physically meaningful terms. From equations (12) and (14)

$$\frac{Q(0)}{\sigma T_b^4}=\frac{1}{N_c}\frac{d^2T^*(0)}{d\xi^2}=\frac{du(0)}{d\xi}$$

and from equation (25)

$$Q(0)=\frac{(\epsilon\sigma T_b^4-\alpha e)\sin^2\theta/2}{\sin^2\theta/2+\alpha\cos^2\theta/2} \tag{31}$$

This relation gives the exact value of the local heat flux and displays no dependence on the conductivity of the material. Since $\alpha B(0)=\epsilon\sigma T_b^4-(1-\alpha)Q(0)$, the local value of the incident and the emitted energy fluxes are given, respectively, by

$$H(0)=\frac{\epsilon\sigma T_b^4\cos^2\theta/2+e\sin^2\theta/2}{\sin^2\theta/2+\alpha\cos^2\theta/2} \tag{32a}$$

$$B(0)=\frac{\epsilon\sigma T_b^4+(1-\alpha)e\sin^2\theta/2}{\sin^2\theta/2+\alpha\cos^2\theta/2} \tag{32b}$$

When $\theta=0$, the contribution from the external source necessarily vanishes and the heat flux vanishes since the incident and emitted energy are equal in magnitude; when $\theta=\pi$, the incident energy is derived solely from the external source. Of special interest are the variations of these functions in the case of small but nonvanishing values of the included angle θ. One would anticipate that if the included angle diminished, and if the absorption and emission coefficients were equal, the emission would approach in the limit black body radiation. The quantitative expression of this fact follows from equation (32b) since

$$B(0)-\frac{\epsilon}{\alpha}\sigma T_b^4\approx\frac{1-\alpha}{\alpha}\frac{\theta^2}{4}\left(e-\frac{\epsilon}{\alpha}\sigma T_b^4\right) \tag{33}$$

applies under conditions for which $\theta^2/4<<\alpha$.

Figure 5 shows the dependence of $Q(0)/(\sigma T_b^4-e)$ on θ and on $\epsilon(=\alpha)$.

In all of the following results the relations $\alpha=\epsilon=1-\rho$ are assumed to hold. Since the case

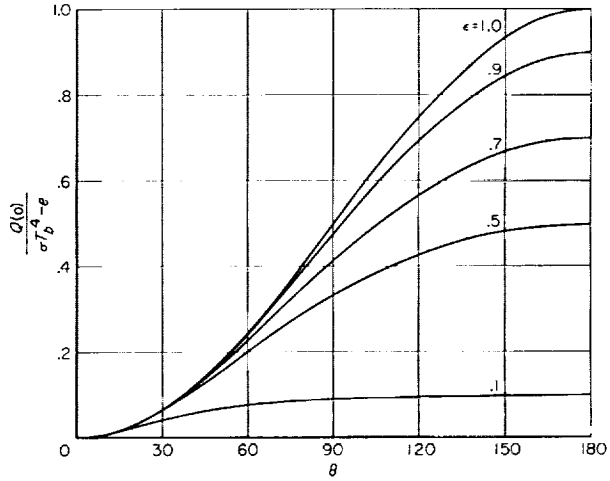

FIGURE 5.—Heat flux at $\xi=0$, with dependence on ϵ and θ.

in which the material surface is held at constant temperature over the entire length is of particular interest, an extensive range of solutions is shown in figure 6. The angle θ has been allowed to increase from 10° to 135° in increments not greater than 10°. These curves extend the calculations of reference 1 and, as remarked previously, may be interpreted so as to yield local heat flux either with or without an external source of radiation. The ordinate scale is the reduced heat flux function $Q^*(\xi)/\epsilon(1-N_e)$ or $Q^*(\xi)/(1-\rho)(1-N_e)$. This form of plotting spreads the curves and makes them easier to read but, even when $N_e=0$, actual magnitudes of the heat fluxes can be compared only after multiplication by the reflectivity factor $1-\rho$. The singularity in the gradient of $Q^*(\xi)$ is not readily apparent from the graphs although the magnitude of the gradient does increase notably as reflectivity increases (emission decreases).

By virtue of the symmetry that was imposed originally in the problem, it is obvious that the results of figure 6 can be applied directly to two-dimensional configurations, such as those shown in figure 7.[1]

The graphs of figure 8 were calculated in order to predict the effect of conductivity on the heat flux, temperature, and thermal current. In all of these cases the external radiation field was deleted, thus $N_e=0$. Although other solutions were calculated, the angle θ has been restricted to three typical cases, 30°, 60°, and 90°. When $N_c=0$ the temperature distribution is uniform, in conformity with infinite conductivity, but the thermal current is finite and not zero. Its value $-2kt\ dT(x)/dx$, as given by Fourier's law, is an indeterminate form but the current must appear in order to support the distribution of local heat flux. The numerical solution was calculated through the use of the independent variable $u(\xi)$ which was directly proportional to thermal

[1] A study of notched radiators with constant wall temperatures has been given by L. F. Daws in a paper entitled The Emissivity of a Groove, British Jour. App. Phys., vol. 5, May 1954, pp. 182-187. This report, which came to the authors' attention during the proofreading of the present paper, tabulates results for $\theta=15°$, 30°, 60°, and $\epsilon=0.64$. Daws also gave an explicit expression for the combined flux at the corner.

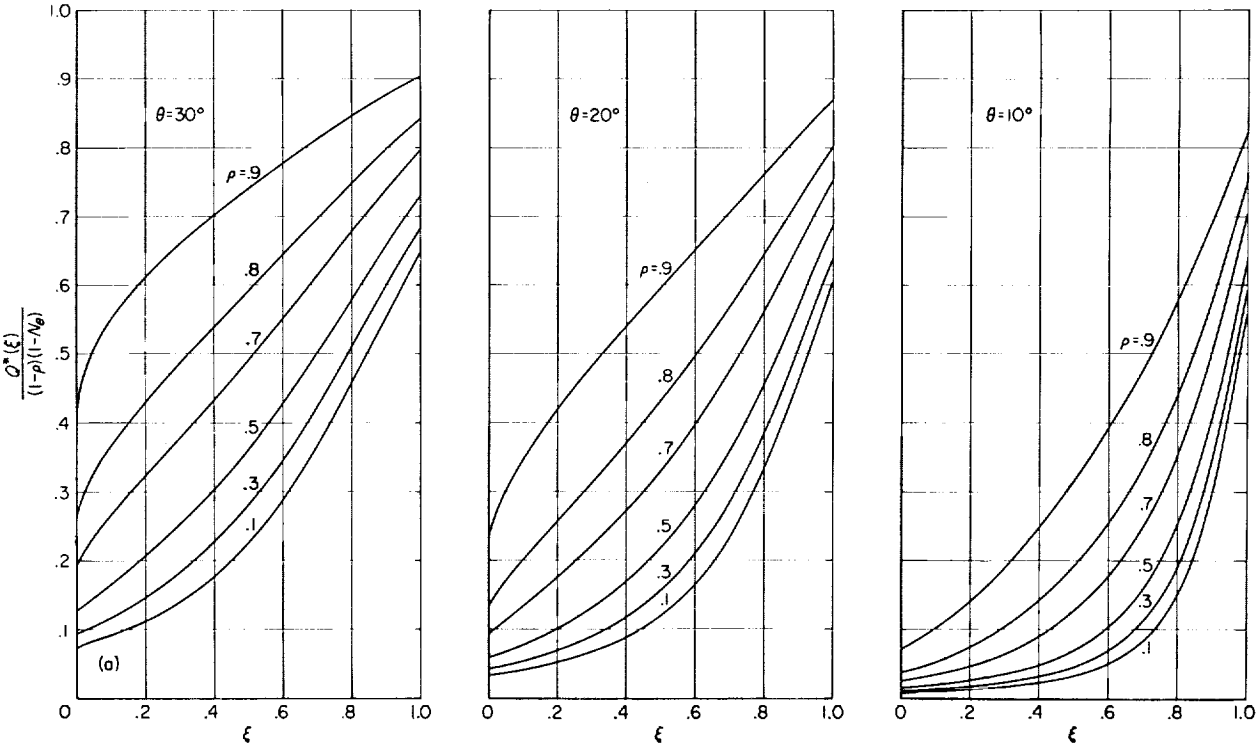

FIGURE 6.—(a)

FIGURE 6.—Local heat flux for constant temperature, with dependence on ρ $(=1-\epsilon)$ and θ.

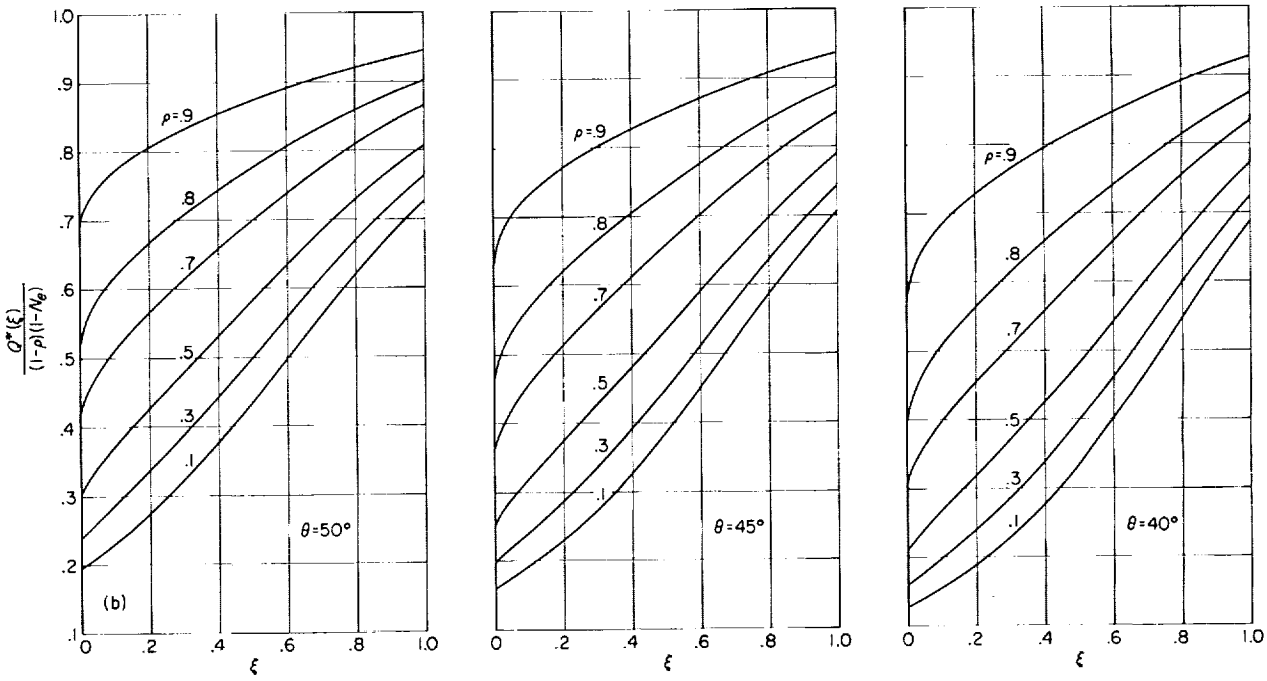

FIGURE 6.—(b) Continued.

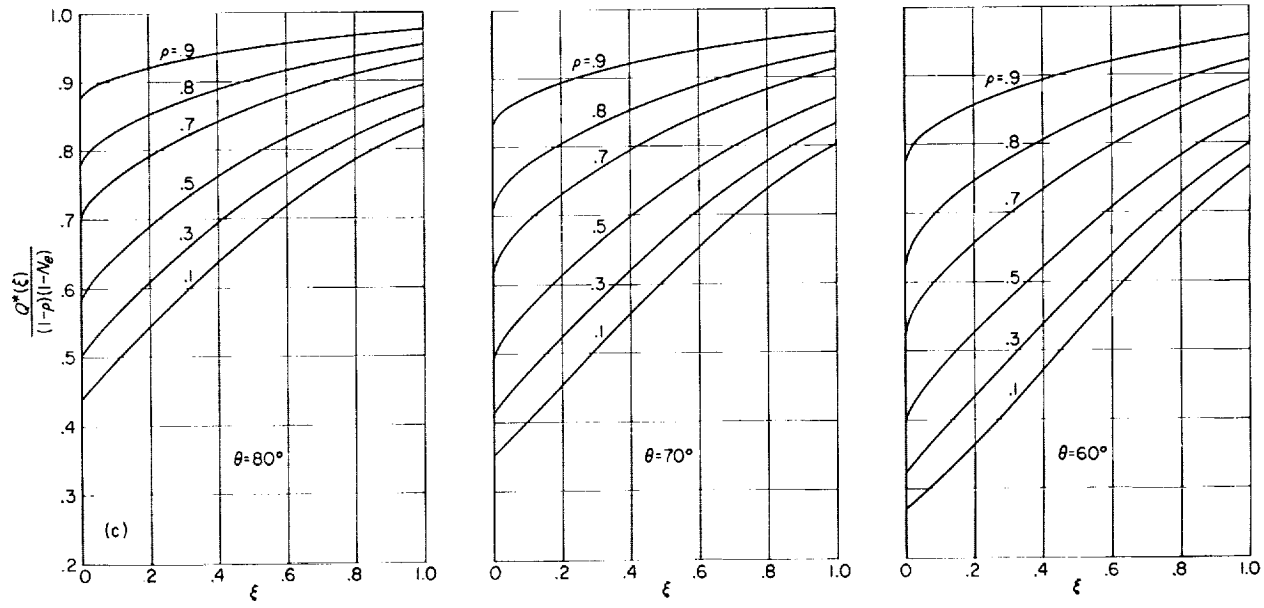

FIGURE 6.—(c) Continued.

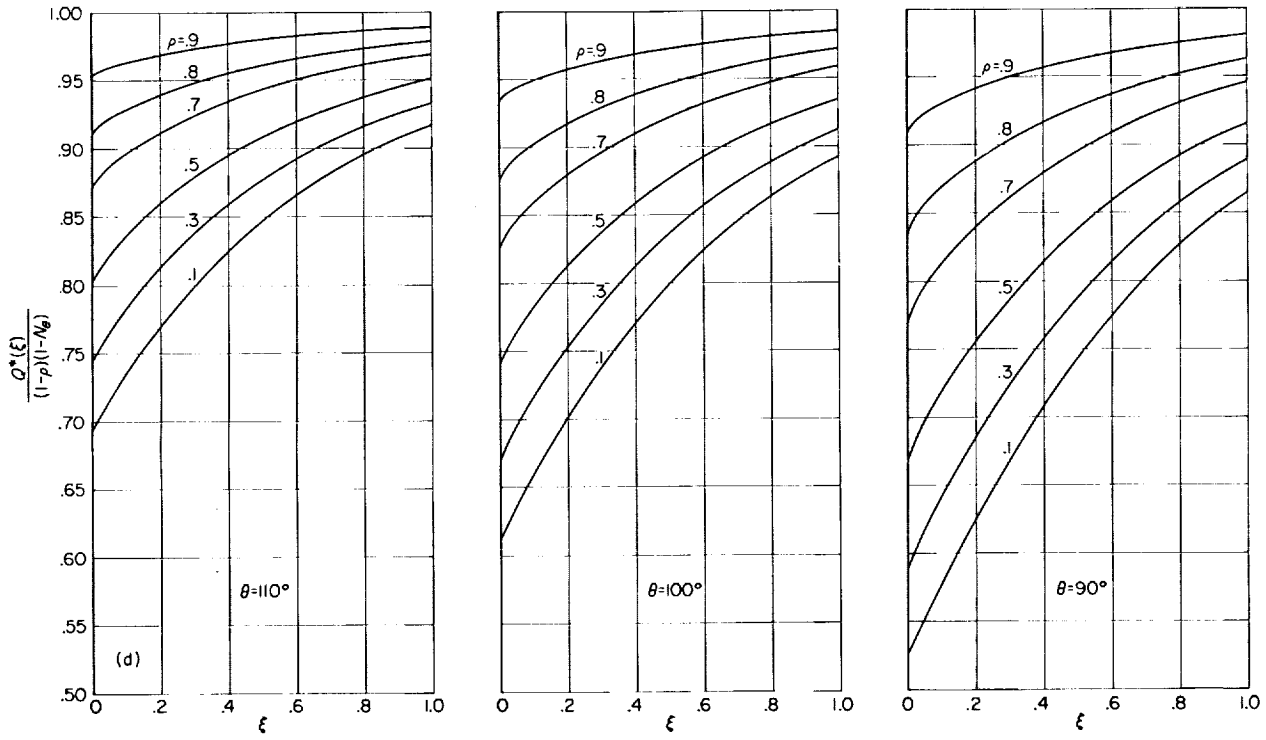

FIGURE 6.—(d) Continued.

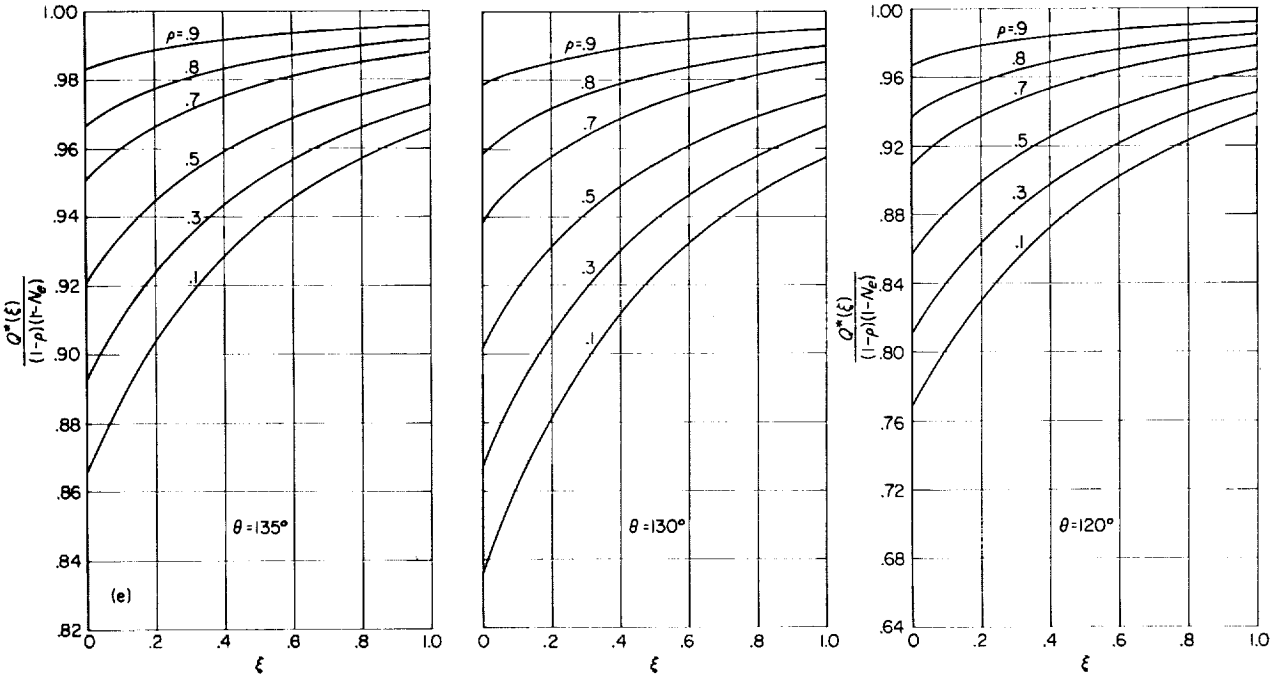

FIGURE 6.—(e) Concluded.

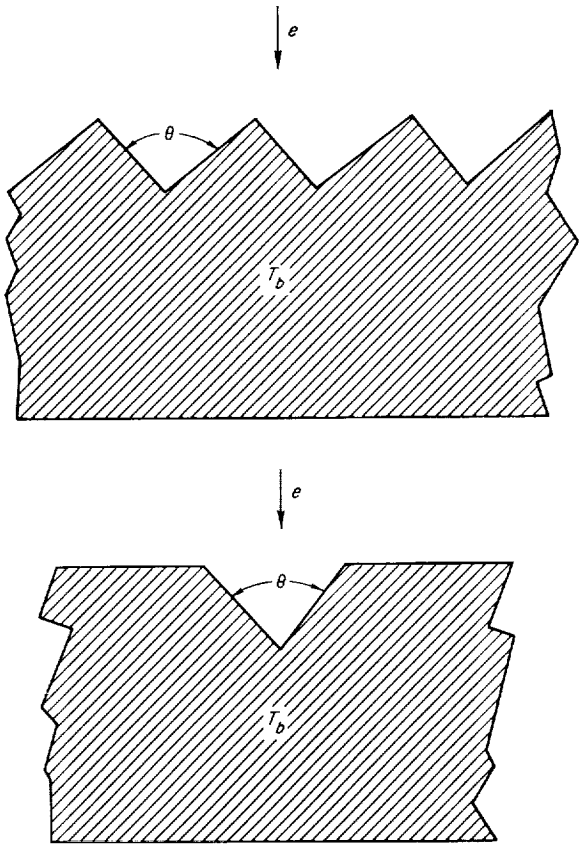

FIGURE 7.—Wedge-shaped cavities in constant-temperature material.

current and the mathematical indeterminacy did not arise in the calculations.

Figure 9 shows the integrated heat flux (see eqs. (13)) corresponding to the results of figure 6. These predictions thus apply to the case of uniform surface temperature. It can be shown directly that the ordinates of the curves at $\epsilon=1$ are given by the expression

$$\left[\frac{\mathscr{Q}^*}{L(1-N_\epsilon)}\right]_{\epsilon=1}=\sin\frac{\theta}{2} \tag{34}$$

It is of some interest, finally, to depart from consideration of the physical predictions and mention an interplay between pure analysis and machine calculations that arises in this particular problem. To illustrate this, consider once more the formal iterative solution of equation (21). The complexity of the analysis can be reduced considerably if, following each new prediction, the unknown function is approximated by a polynomial of increasing order.

Suppose in equation (21), the function $B_I^*(\xi)$ is a constant C. Then

$$C=1+C\frac{(1-\alpha)}{2}\left[1+\frac{a-\xi}{(1-2a\xi+\xi^2)^{1/2}}\right]$$

Agreement at $\xi=0$ demands that

$$B_I^*(0)=C_0=\left[1-\frac{(1-\alpha)(1+a)}{2}\right]^{-1}$$

If the constant is again forced to give agreement at $\xi=1$, one gets

$$B_I^*(1)=C_1=\left[1-\frac{(1-\alpha)}{2}\left(1-\sqrt{\frac{1-a}{2}}\right)\right]^{-1}$$

A linear approximation can thus be written in the form

$$B_I^*(\xi)\approx C_0+(C_1-C_0)\xi$$

and a new prediction calculated. Such a calculation gives

$$\begin{aligned}B_I^*(\xi)\approx 1&+\frac{(1-\alpha)}{2}C_0\left[1+\frac{a-\xi}{(1-2a\xi+\xi^2)^{1/2}}\right]\\&+\xi(C_1-C_0)\frac{(1-\alpha)(1-a^2)}{2}\\&\left\{\frac{1}{(1-a^2)}\left[\frac{2a^2-1-a\xi}{(1-2a\xi+\xi^2)^{1/2}}+a\right]\right.\\&\left.+\ln\frac{[(1-a\xi)+(1-2a\xi+\xi^2)^{1/2}]}{\xi(1-a)}\right\}\end{aligned} \tag{35}$$

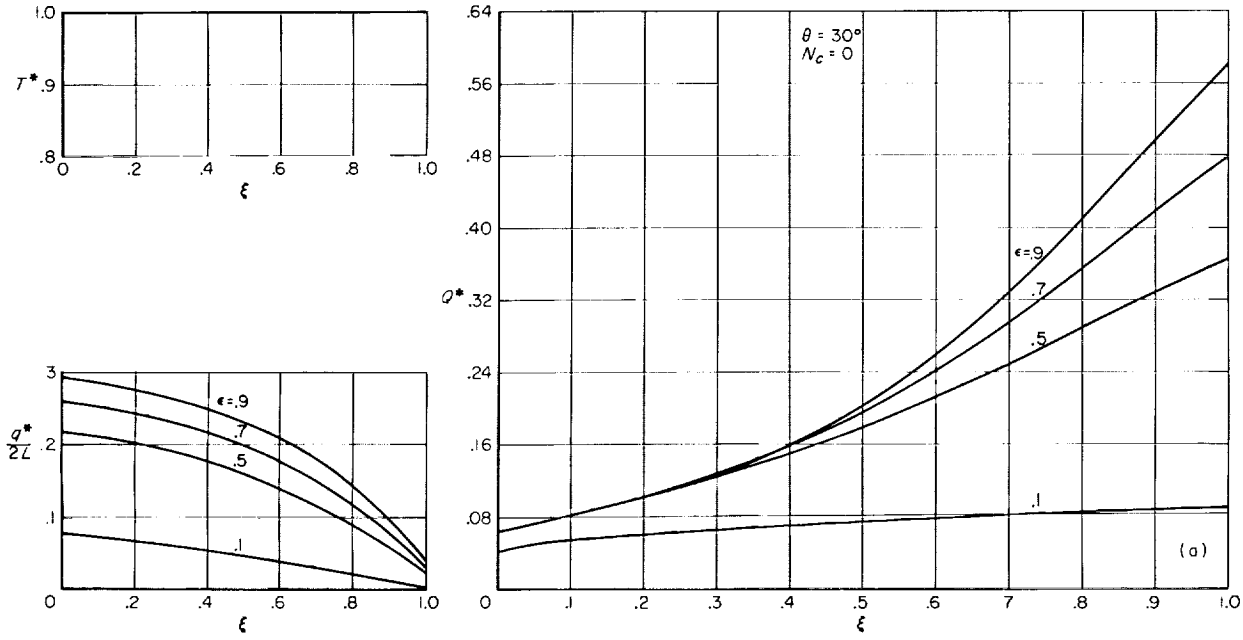

FIGURE 8.—(a).

FIGURE 8.—Temperature, thermal current, and temperature distributions in conducting planar fins; $t/L=0.05$.

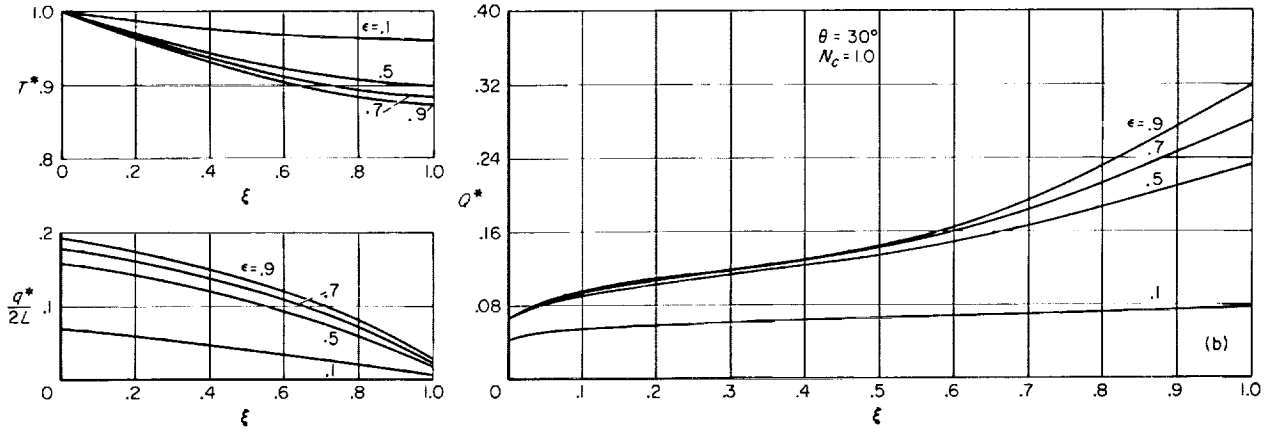

FIGURE 8.—(b) Continued.

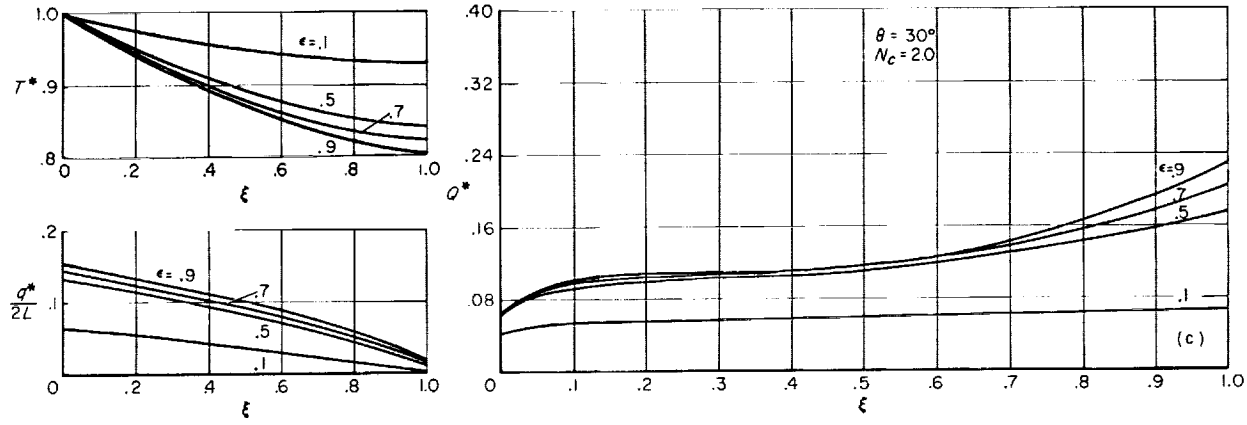

FIGURE 8.—(c) Continued.

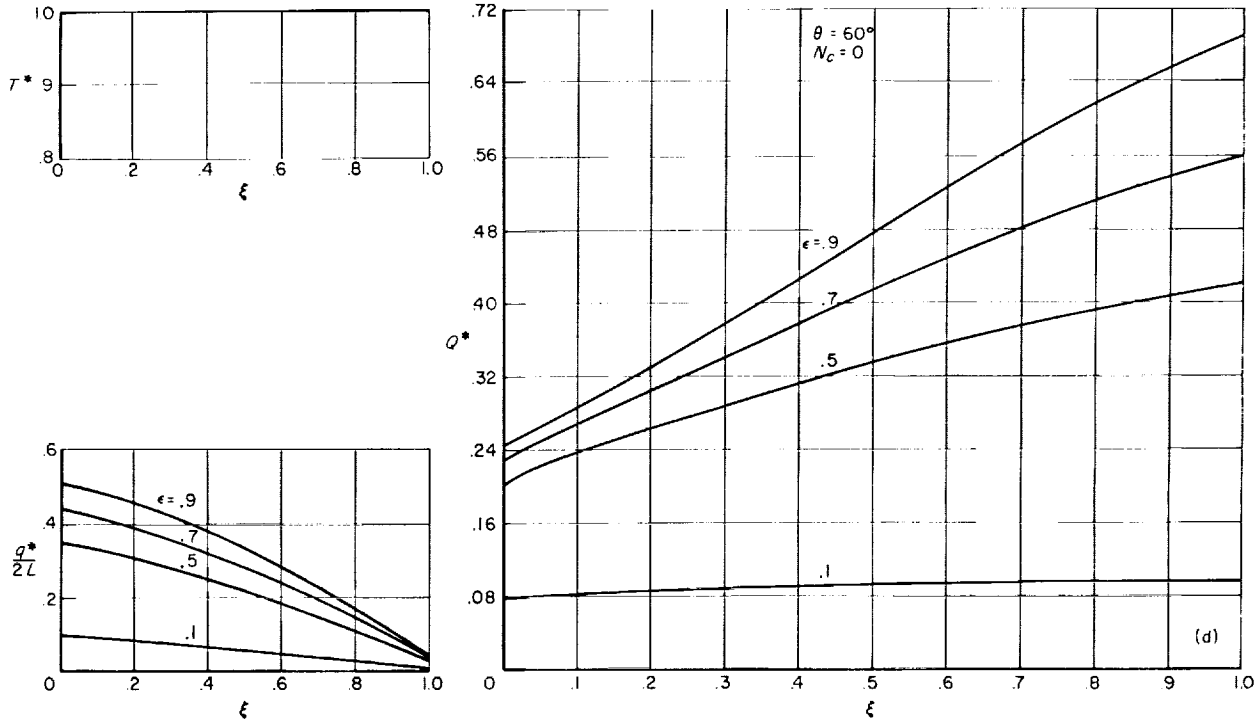

FIGURE 8.—(d) Continued.

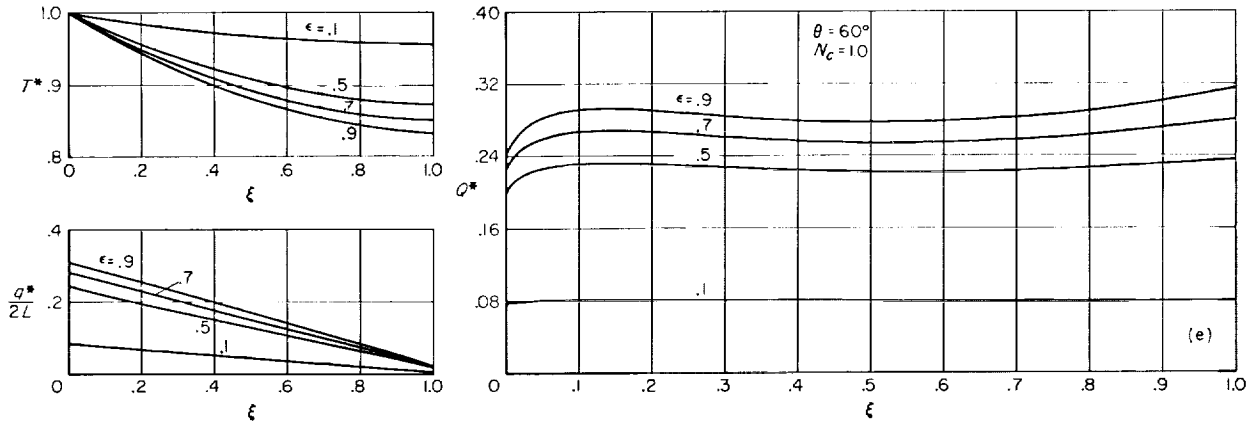

FIGURE 8.—(e) Continued.

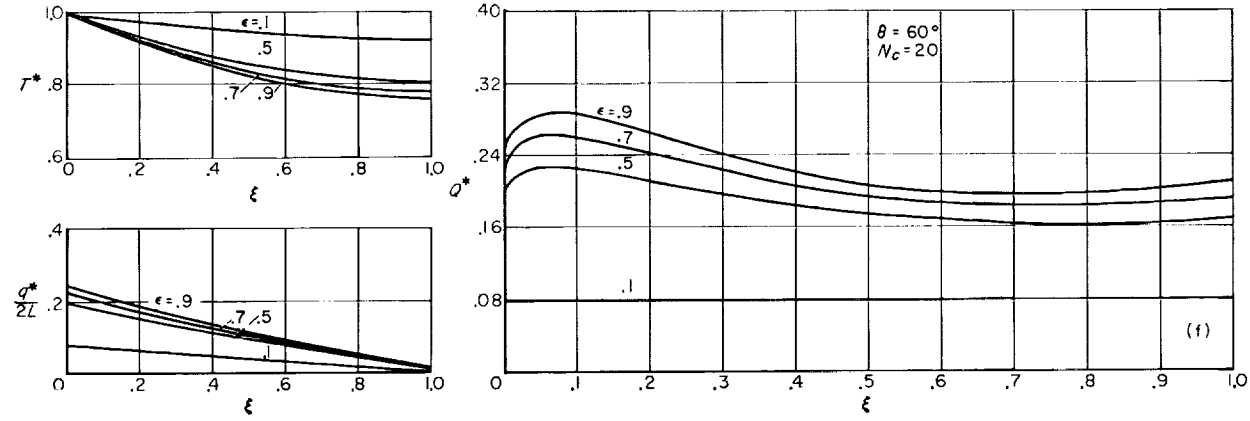

FIGURE 8.—(f) Continued.

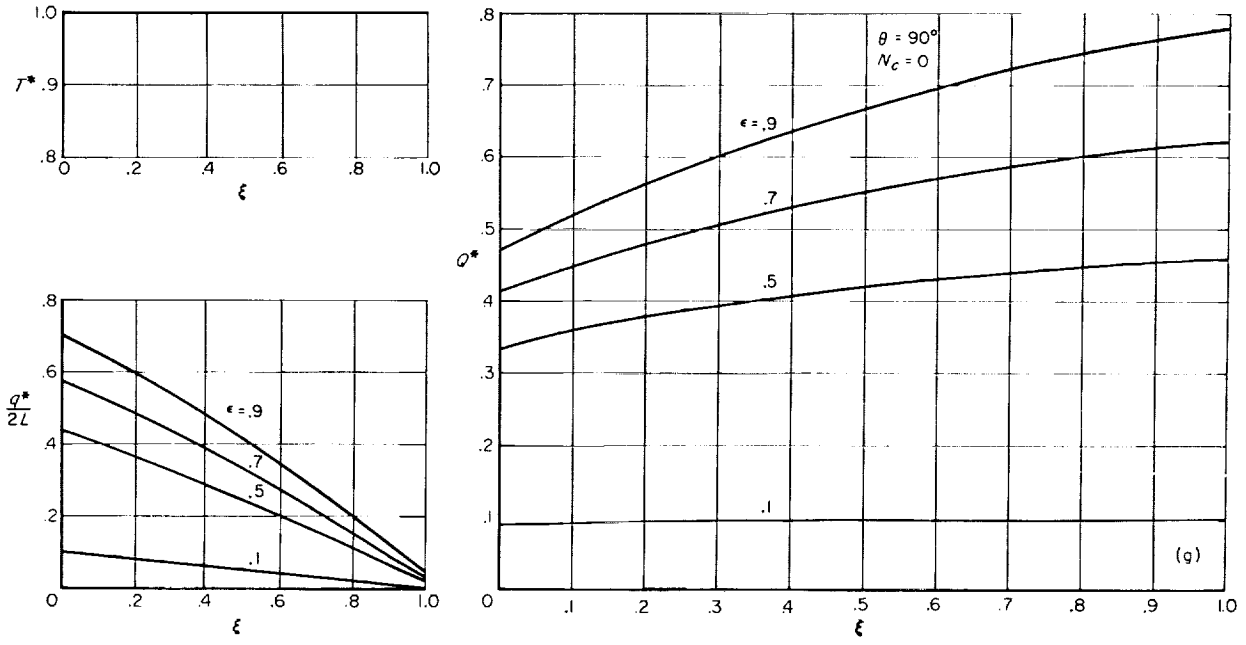

FIGURE 8.—(g) Continued.

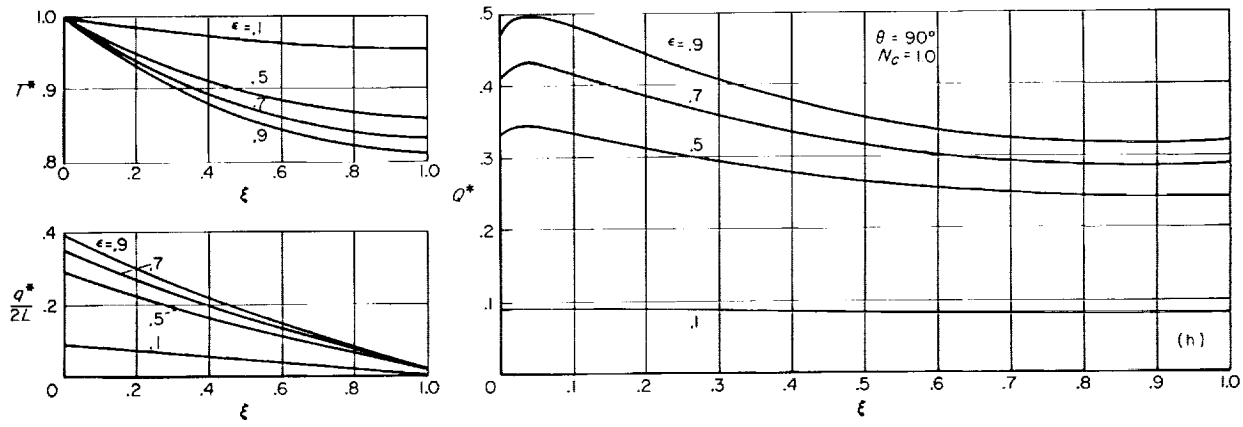

FIGURE 8.—(h) Continued.

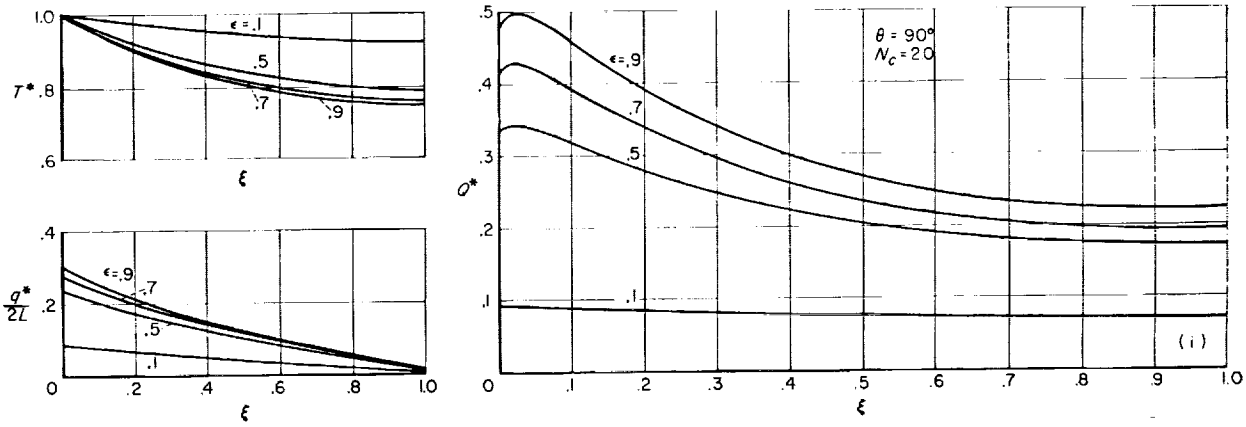

FIGURE 8.—(i) Concluded.

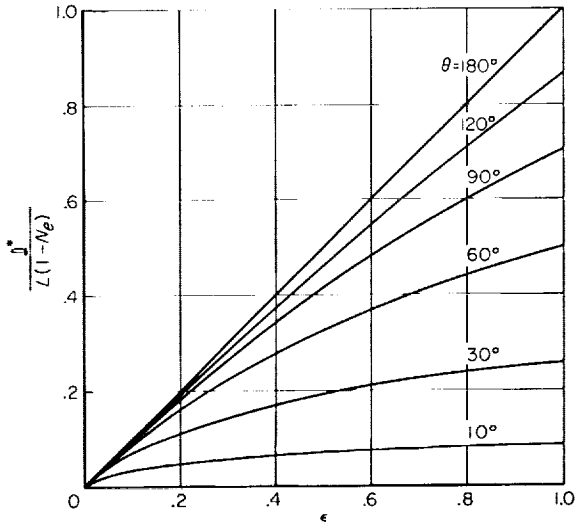

FIGURE 9.—Integrated heat flux for constant temperature, with dependence on ϵ and θ.

In order to continue the process, values at $\xi=0$, 0.5, and 1 can be determined and $B_l^*(\xi)$ approximated by a parabola passing through the known ordinates.

The principal idea being developed here is that analytical procedures like the one above can be studied experimentally in combination with numerical results and the range of validity of the approximate predictions then determined. Figure 10 shows a comparison between exact results and predictions based on equation (35) for the special case in which $\theta=90°$. Considering the roughness and simplicity of the approximations used, the agreement is surprisingly good. At $\theta=10°$ the agreement is wholly inadequate but relations like equation (35) may serve a useful purpose when some sacrifice in accuracy is acceptable and the range of the parameters is limited.

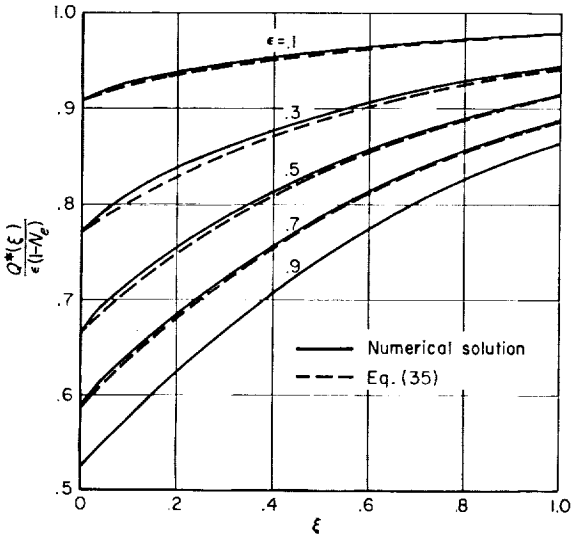

FIGURE 10.—Comparison between exact and approximate prediction of local heat flux, $\theta=90°$.

NUMERICAL METHODS

The discussion in this section concerns the methods and analysis used to solve equation (17a) for the given boundary conditions by means of a digital computing machine. Its inclusion in a report of this kind has been brought about by the development of computer "languages" (such as FORTRAN), by means of which the engineer can communicate directly with the machine. The experience of the authors has been that an understanding of such languages considerably affects the kind of theoretical analysis the engineer directs toward the solution of a specific problem; turning it toward points that arise principally because a machine is to be used, and away from points (which, without the machine, might have consumed large anounts of time) that are no longer essential. Their experience has also been that such knowledge is extremely useful in the formulation of the problem, permitting the engineer to recognize at that critical stage just what assumptions and compromises are and are not really necessary in that these decisions affect machine running time by orders of magnitude.[2]

The numerical study of the present problem requires special attention in two areas, one, the numerical treatment of the singularity in the kernel, and the other, the production of a program that produces a solution to the integro-differential equation in a short time. The latter depends, of course, on the number of runs anticipated. In this problem, for each θ there are five parameters N_c, N_e, t/L, α, and ϵ, and a very modest coverage of them all demands a large number of individual solutions. The manner in which these difficulties were treated will now be considered.

The difficulty at the singularity ($\xi=\eta=0$ in eq. (9)) was largely overcome when the exact value of the unknown was discovered there, see equation (25). The essentials of the remaining analysis are as follows.

Equation (18a) was written in the form

$$\frac{du(\xi)}{d\xi}=G(\xi)+\frac{(1-\alpha)(1-a^2)}{2}\int_0^1 A(\eta)K(\xi,\eta)d\eta \tag{36}$$

where

$$A(\eta)=\frac{du(\eta)}{d\eta}-\frac{G(\eta)}{1-\alpha}$$

and $G(\xi)$ is given by equation (18b). The length from 0 to 1 was then divided into $(M-1)$ equally spaced intervals. In each interval $A(\eta)$ was replaced by a straight line. Thus, if $A_N=A[(N-1)/(M-1)]$

$$\begin{aligned} I(\xi)&=\int_0^1 A(\eta)K(\xi,\eta)d\eta \\ &\cong\sum_{N=1}^{M-1}\int_N^{N+1}\{[N-(M-1)\eta]A_N \\ &\quad+[(M-1)\eta-N+1]A_{N+1}\}K(\xi,\eta)d\eta \end{aligned} \tag{37}$$

The integrals $\int K(\xi,\eta)d\eta$ and $\int \eta K(\xi,\eta)d\eta$ are easily evaluated. The coefficient for the known $A_1=A(0)$ was determined by calculating the integrals for nonzero ξ, then setting $\eta=0$ and then letting ξ go to zero. This simple approximation resulted in terms which presented no numerical difficulties in any region. The estimated error, based on runs with differing M, is less than can be shown on any of the graphs in this paper.

MACHINE TIME

The decision was made at the outset to use a method of iteration to attack the present problem. This choice was made for a variety of reasons. In

[2] The engineer can at least be aware of the approximate minimum time a really optimum programming of his problem requires. This is based largely on the number of independent variables in his particular problem and the range of parameters he wishes to cover. How close he chooses to approach this minimum depends upon his breadth of interest and his particular economy.

the first place an analysis (eqs. (26) and the following) had already shown such a method converges. Secondly, iterative methods are easy to control. They can be terminated quickly if they are diverging, and, if their convergence is slow, methods can be brought to bear that will often greatly hasten it. Finally, in the present case, an iterative program is quite easy to write and, therefore, comparatively easy to put into production without excessive delay.

Having chosen the iterative technique, and having in mind a large number of cases to study, it was considered necessary to estimate the minimum feasible time required for each new iterative solution. The crux of the problem here is the time required to evaluate the integral $I(\xi)$ given by equation (37). If $i(\xi)$ is calculated at the same points as $A(\eta)$, we can write

$$I_J = I\binom{J-1}{M-1} \cong \sum_{N=1}^{M} A_N H_{JN},\ J=1,2,\ldots,\ldots,M \tag{38}$$

The time required to calculate the M different values of I_J is given by the product $M^2\times\tau\times\mu$ where μ is the unit machine time (12×10^{-6} sec for an IBM 704) and τ is the number of machine units required for calculating one $A_N H_{JN}$ and adding it to the others. Iteration times are clearly minimized if H_{JN} is calculated only once (several hundred machine units are required to find each H_{JN}) and stored in the machine for subsequent use.[3] The value of τ for an IBM 704 is then about 35 and the time required to calculate the set of I_J's for each iterative solution is about $420\times M^2\times10^{-6}$ seconds. Of course, the complete iteration demands additional calculations but they involve only one independent variable and are, therefore, proportional to M, not M^2 (see table 1). Allowing that they double the above figure, the total time for one iteration amounts to around $840\times M^2$ microseconds, or about 2.2 seconds for $M=51$, the value generally used in this report.

In actual practice slightly over 300 different cases were run, about a quarter of which are shown in this report. The production time was just under 2 hours.[4] About nine iterations were required for the average production case [5] which accounts for 85 percent of the production time on the basis of the 2.2-second estimate. The rest of the time is roughly accounted for by the necessary data input and output and the evaluation of the H_{JN} each time θ was changed.

Table 1. Estimates of minimum times involved for certain operations on an IBM 704 (assuming $G_0(\xi)$ and $G_1(\xi, x)$ have been properly weighted and stored). Both ξ and x take M values in the interval 0 to 1.

$\int_0^1 G_0(\xi) f(\xi) d\xi \sim 380\ M\times10^{-6}$ seconds
$\int_0^x G_0(\xi) f(\xi) d\xi,\ 0\le x\le 1 \sim 1000\ M\times10^{-6}$ seconds
$\int_0^1 G_1(\xi, x) f(\xi) d\xi,\ 0\le x\le 1 \sim 420\ M^2\times10^{-6}$ seconds

[3] This requires M^2 words in storage but offers no problem if $M\le51$ even for a machine limited to an 8000 word capacity.

THE ITERATIVE PROCEDURE

In carrying out a numerical iteration some test must be provided to decide when the iterations can be terminated. In this report a solution is assumed to have been arrived at when the integral of the absolute value of the difference between two successive iterative solutions drops below a certain limit. In particular, when

$$\int_0^1 \left|\left(\frac{du}{d\xi}\right)_J - \left(\frac{du}{d\xi}\right)_{J+1}\right| d\xi = \sum_I^M WT(N)\,|DU1(N)-DU2(N)| \le 0.0001 \tag{39}$$

where $WT(N)$ is in integration weight (e.g., $\Delta h/3$ times 1, 4, 2, 4, . . ., 2, 4, 1 if Simpson's rule is used) and $DU1(N)$ and $DU2(N)$ are arrays holding two consecutive iterations. The first iterative technique used is outlined below:

1. Input general data.
2. Prepare arrays for simple integrals.
3. Input θ.
4. Calculate and array the kernel $K(\xi, \eta)$ in equation (36).
5. Input ϵ, N_c, t/L, and S and evaluate permanent constants.
6. Calculate right-hand side of equation (18a), assuming G and $du/d\xi$ are the constants given by equations (25) and (18b) with $\xi=0$. Array the results in $DU1(N)$, $1\le N\le M$.
7. Input N_c.

[4] Total time, including compiling and checkout, was 3.61 hours.

[5] This has been considerably improved for future work. Eight cases that took 208 iterations were rerun using a method for accelerating convergence and the number was reduced to 60. This method is discussed in the following sections.

8. Calculate the right-hand side of equation (18b) using $DU1(N)$. Array the result in $G(N)$.
9. Calculate the right-hand side of equation (18a) using the values now in $DU1(N)$ and $G(N)$. Array in $DU2(N)$.
10. Find $\int_0^1 |DU1-DU2|d\xi$. Store result in array ERROR (I).
11. If ERROR $(I) \leq 0.0001$ take instruction 13, otherwise take 12.
12. Replace $DU1(N)$ with $DU2(N)$ and return to 8.
13. Output data and return to 3, 5, or 7.

The procedure just presented was satisfactory for the study of variations of the remaining parameters, N_c, ϵ, t/L, and θ. A typical plot of the ERROR term against the number of iterations is shown in figure 11.

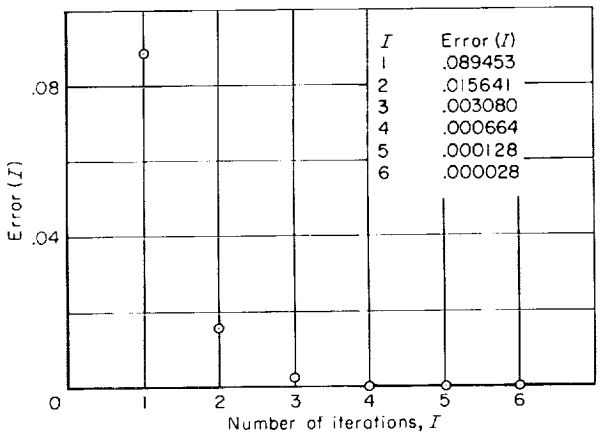

FIGURE 11.—Typical variation of error term with number of iterations.

A METHOD FOR ACCELERATING CONVERGENCE

Although figure 11 was typical of most cases, two regions of parametric combinations converge very slowly using the above method. Both occur for all values of t/L considered. One occurs when N_c, ϵ, and θ take their largest values and the other, when ϵ and θ are small throughout the entire range of N_c.

Often the successful application of a converging iteration scheme depends upon the first choice of the dependent variable. A poor first choice can result in an intolerably slow rate. This is precisely what happened in the present study when t/L, N_c, ϵ, and θ were equal to 0.05, 2, 0.9, and 120°, respectively. The circled dots in figure 12 show the variation of the ERROR term for 30 iterations. Obviously the convergence rate is unacceptable. Detailed inspections of the situation are presented in figures 13 and 14. Figure 13 shows the initial choice of $du/d\xi$ and the first five successive iterations. Figure 14 shows the value of $du/d\xi$ at $\xi=1$ for the first 20 iterations. In both cases the final value is given for comparison.

Fortunately, the kind of convergence illustrated in these sketches can be improved remarkably by means of methods developed for that purpose (e.g., see refs. 3, 4, 5, 6). All of the referenced methods are based on the assumption that a sequence of terms in an iteration contain information

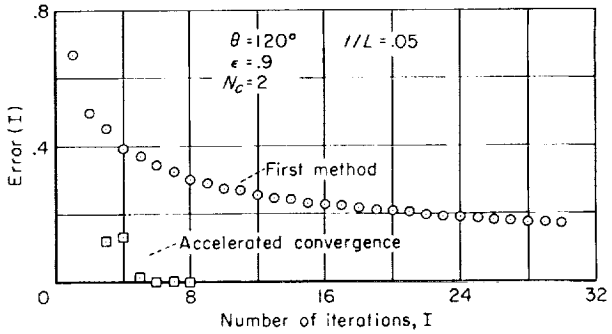

FIGURE 12.—Slowly converging iteration series and improvement brought about by a method for accelerating convergence.

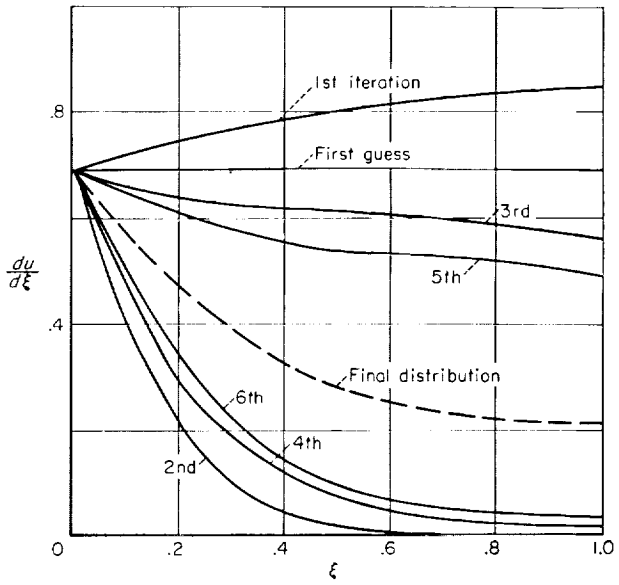

FIGURE 13.—First few iteration distributions of $du/d\xi$ against ξ for slowly converging case.

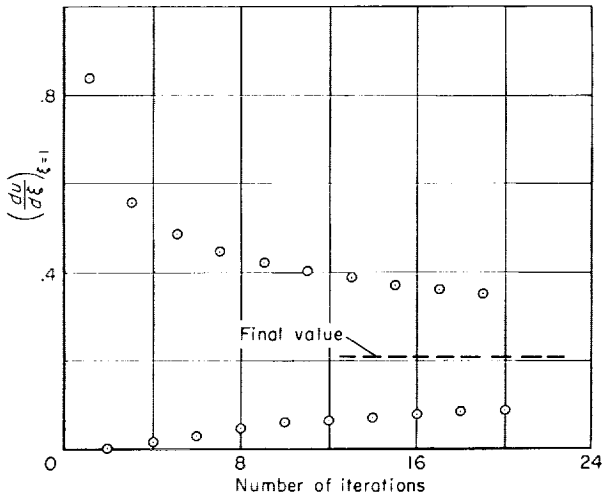

FIGURE 14. Variation of end points, first few of which are shown in figure 13, for 20 iterations.

regarding their final value, information which is lost if only the last term is used for each successive step. To apply these methods a few consecutive iterative solutions are retained in the machine memory and eventually called upon to form the final estimate or to find an improved starting value for a new series of iterations. Shanks (ref. 3) has developed a method for using any number of iterative solutions. In this report only three are used.

We can describe the method used herein geometrically with the aid of figure 15. Consider

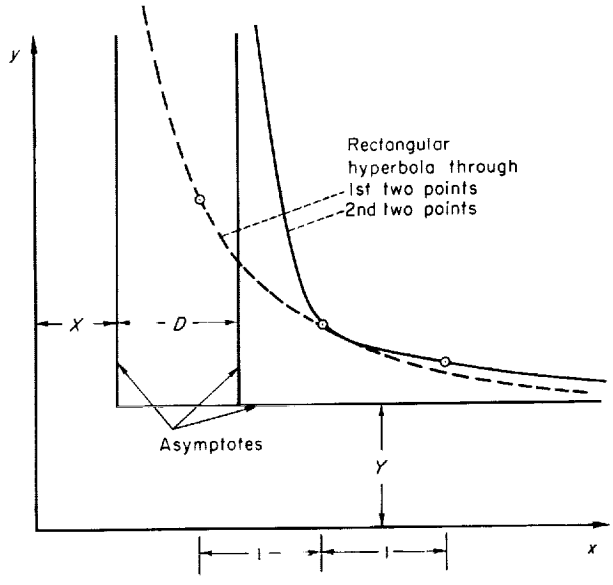

FIGURE 15.—Rectangular hyperbolas mentioned in discussion.

three successive points y_1, y_2, y_3 in any iterative scheme and plot them against, say, x with unit spacing. Pass a rectangular hyperbola through the first two, and another with the *same y asymptote* through the second two, but, for generality, with an x asymptote displaced by D. Thus

$$(X-x_1)(Y-y_1)=c$$
$$(X-x_2)(Y-y_2)=c$$

and

$$(X+D-x_2)(Y-y_2)=c^*$$
$$(X+D-x_3)(Y-y_3)=c^*$$

are the equations which must be satisfied. The difference between the two equations in each case [6] gives, for a fixed D, two equations for the unknowns X and Y. Solving for Y and using the relations $x_1-x_2=x_2-x_3=1$, one finds

$$\frac{Y-y_3}{y_2-y_3}=1-(2-D)\left(1-\frac{y_2-y_3}{y_1-y_2}\right)^{-1} \qquad (40)$$

The variable Y is a point on the curve that will form the starting distribution for the next iteration. Its distance from the last approximation divided by the distance between the last two approximations, $(Y-y_3)/(y_2-y_3)$, is itself a rectangular hyperbola when considered as a function of the variable $(y_1-y_2)/(y_2-y_3)$. This is illustrated in figure 16.

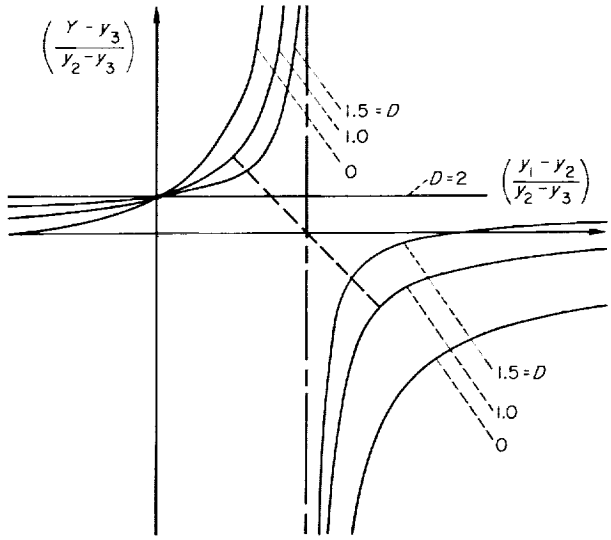

FIGURE 16. Illustration of equation (34), formula used to accelerate convergence.

[6] Notice that, by considering only the differences, the final formula will be independent of c and c^*. Notice also that the sketch represents a very simplified picture of what can happen. Both branches of both hyperbolas (which can lie in any quadrant since c and c^* can be either + or −) are often involved. The latter is the case, for example, when applying the results to the points in figure 14.

We turn now to the choice of D. If three points are actually spaced as shown in figure 15, a "best" generally acceptable D is not resolved. Values of D between 0 and 1.5, say, yield equations that could give the proper limiting Y. If, on the other hand, the first and third points are nearly equal and the second is considerably different from them, as is the case in figure 14, the best D for our purposes is readily determined. In such cases the choice $D=0$ yields a value for Y that is nearly equal to the first and third y. The choice $D=2$ yields a value equal to the second y. The choice $D=1$ yields a value nearly half way between, and since we are *assuming* that the sequence of points is similar to that shown in figure 14 (i.e., converging, although, perhaps, slowly), this choice is clearly preferable. It is significant that when $D=1$, equation (40) is identical to the expression used by several authors (a few of which are referenced at the beginning of this section) to accelerate convergence.[7]

Let us briefly consider the real value of equation (40) for use in the iterative solution to equations like those given by (18). At once, it appears that equation (40) can only be useful if three successive terms do actually contain information about the value they eventually approach; but in equation (18) each point in any iteration is linked in a complex, nonlinear way with every other point. Hence, a sequence of iterative solutions for one point may have quite valuable information regarding their limit, whereas a companion sequence for another point may contain no information whatsoever. Three points that lie (to some numerical degree of accuracy) on a straight line, for example, have no value in determining a bounded asymptote (provided one exists). For this reason equation (40) was not used to evaluate Y in the vicinity $(y_1-y_2)/(y_2-y_3)\approx 1$, the region where three successive points approach a linear relationship. In fact, the scheme finally chosen to accelerate convergence was to use equation (40) with $D=1$ for

$$0.5\geq\frac{y_1-y_2}{y_2-y_3}\geq 1.5$$

and

$$\frac{Y-y_3}{y_2-y_3}=1-\frac{y_1-y_2}{y_2-y_3} \qquad (41)$$

[7] It is interesting to note that Isakson (ref. 4) derives equation (40) for $D=1$ by fitting to three successive points a curve that approaches its asymptote exponentially.

in the interval between 0.5 and 1.5 (the latter amounts to the straight dashed line shown in figure 16).

In terms of the machine, this required a modification to the program outlined above. At the beginning of step 12, $DU1$ and $DU2$ were stored in two new arrays the first (or every odd) time through. The second (or every even) time, $DU2$ was stored in a third array and a subroutine was entered which calculated a new $DU1$ on the basis of equation (40) or (41). The machine was then, again, sent back to step 8.

RESULTS OF ACCELERATING CONVERGENCE

When the method presented in the preceding section was applied to the case $t/L=.05$, $N_c=2$, $\epsilon=0.9$, and $\theta=120°$, the results for which, by the first method, are shown in figures 12, 13, and 14, the sequence of ERROR terms were those given in figure 17 and also, for comparison, in figure 12.

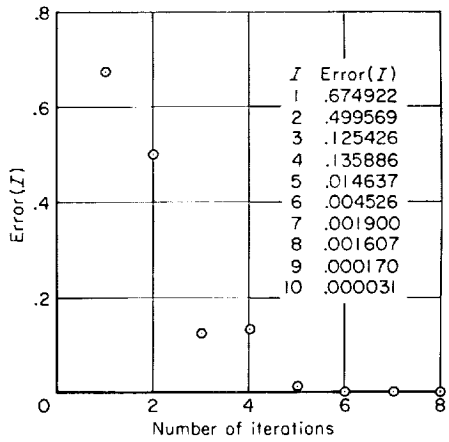

FIGURE 17.—Variation of error term after accelerated convergence method had been applied to slowly converging series.

The final values, after 10 iterations, are the dashed curves in figures 13 and 14. The success of the method in this case is evident.

The second region of poor convergence, small ϵ and small θ, was not significantly improved by the above technique. Figure 18 shows the first three iterations (after the initial choice of a constant equal in magnitude to the starting value), and the final distribution. The first "improved" curve is given by the dashed line and shows a discontinuity between 0.82 and 0.84. It is at this point that the

machine switches from equation (40) to (41). It is our hypothesis, therefore, that for ξ less than 0.84, the first three iterations have lost most of

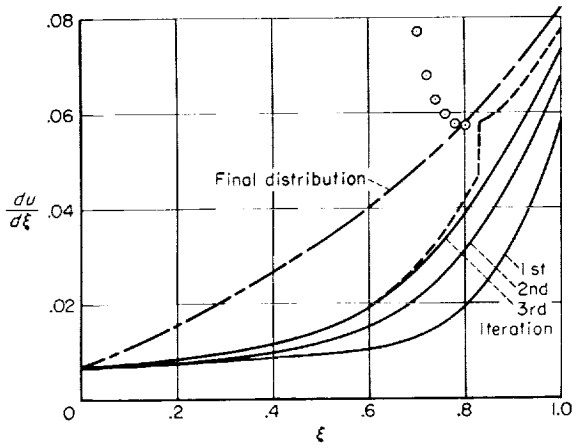

FIGURE 18. Illustration of three slowly converging iterations and "improved" distribution obtained from them.

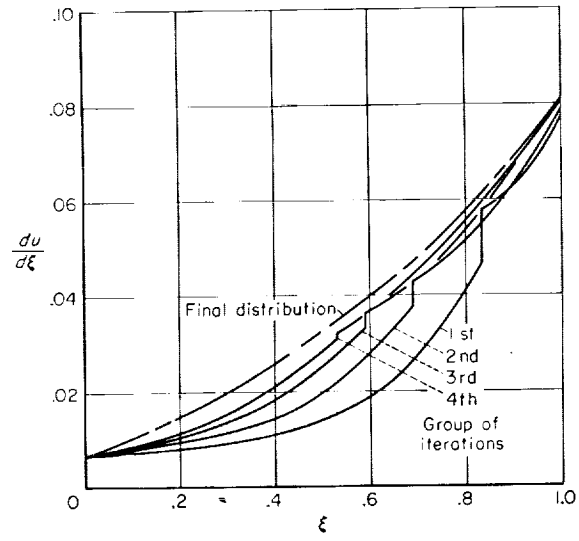

FIGURE 19.—Successive "improved" iterations resulting from application of accelerating convergence technique to slowly converging process.

their value insofar as predicting their asymptote is concerned. To substantiate this, equation (40) was applied to calculate points for lower ξ. The results are shown in figure 18 down to $\xi=0.7$ by the circled dots. Below 0.7 the values were negative! For this case, at least, the hypothesis is correct.

In spite of the above difficulties, the method was continued and the iterations converged (in the sense that condition (39) was satisfied) in 20 steps. For the same accuracy 21 steps were required by the first method. Figure 19 shows the first four new successive sets of three iterations. The number of points containing significant information regarding their limit according to the above criterion gradually increases, the dividing line moving toward the origin like a wave with diminishing amplitude.

Ames Research Center,
National Aeronautics and Space Administration,
Moffett Field, Calif., *May 16, 1961.*

REFERENCES

1. Sparrows, E. M., Gregg, J. L., Szel, J. V., and Manos, P.: Analysis, Results, and Interpretation for Radiation Between Some Simply-Arranged Gray Surfaces. Jour. of Heat Transfer, Ser. C, Trans. ASME vol. 83, 1961, pp. 207–214.
2. Eckert, E. R. G., Irvine, T. F., Jr., and Sparrow, E. M.: Analytic Formulation for Radiating Fins With Mutual Irradiation. ARS Jour., vol. 30, no. 7, July 1960, pp. 644–646.
3. Shanks, Daniel: Non-Linear Transformations of Divergent and Slowly Convergent Sequences. Jour. Math. and Phys., vol. 34, Apr. 1955, pp. 1–42.
4. Isakson, Gabriel: A Method for Accelerating the Convergence of an Iterative Procedure. Jour. Aero. Sci., vol. 16, no. 7, July 1949, p. 443.
5. Aitken, A. C.: On Bernoulli's Numerical Solution of Algebraic Equations. Proc. Roy. Soc. Edinburgh, vol. 46, 1926, pp. 289–305.
6. Hartree, D. R.: Notes on Iterative Processes. Cam. Phil. Soc., vol. 45, pt. 2, Apr. 1949, pp. 230–236.

U.S. GOVERNMENT PRINTING OFFICE: 1962

NASA TR R-116
National Aeronautics and Space Administration.
NUMERICAL PREDICTIONS OF RADIATIVE INTERCHANGE BETWEEN CONDUCTING FINS WITH MUTUAL IRRADIATIONS. Max. A. Heaslet and Harvard Lomax. 1961. i, 22 p. diagrs., tab. GPO price 35 cents. (NASA TECHNICAL REPORT R-116)

Analytical and numerical methods are developed that predict the flux of radiant energy from a family of thin, planar, conducting fins. For a symmetrical array of fins, extending out from a common edge, conducting heat internally, and radiating diffusely, a nonlinear integro-differential equation is derived and solved. Specific results are given for parametric variations of conduction, emissivity, fin geometry, and base temperature. The techniques of calculation are studied with possible extensions in mind.

(Initial NASA distribution; 2, Aerodynamics, missiles and space vehicles; 26, Materials, other; 27, Mathematics; 33, Physics, theoretical; 35, Power sources, supplementary; 37, Propulsion system elements; 47, Satellites; 51, Stresses and loads; 52, Structures.)

Copies obtainable from Supt. of Docs., GPO Washington

I. Heaslet, Max. A.
II. Lomax, Harvard
III. NASA TR R-116

NASA

NASA TR R-116
National Aeronautics and Space Administration.
NUMERICAL PREDICTIONS OF RADIATIVE INTERCHANGE BETWEEN CONDUCTING FINS WITH MUTUAL IRRADIATIONS. Max. A. Heaslet and Harvard Lomax. 1961. i, 22 p. diagrs., tab. GPO price 35 cents. (NASA TECHNICAL REPORT R-116)

Analytical and numerical methods are developed that predict the flux of radiant energy from a family of thin, planar, conducting fins. For a symmetrical array of fins, extending out from a common edge, conducting heat internally, and radiating diffusely, a nonlinear integro-differential equation is derived and solved. Specific results are given for parametric variations of conduction, emissivity, fin geometry, and base temperature. The techniques of calculation are studied with possible extensions in mind.

(Initial NASA distribution: 2, Aerodynamics, missiles and space vehicles; 26, Materials, other; 27, Mathematics; 33, Physics, theoretical; 35, Power sources, supplementary; 37, Propulsion system elements; 47, Satellites; 51, Stresses and loads; 52, Structures.)

Copies obtainable from Supt. of Docs., GPO Washington

I. Heaslet, Max. A.
II. Lomax, Harvard
III. NASA TR R-116

NASA

NASA TR R-116
National Aeronautics and Space Administration.
NUMERICAL PREDICTIONS OF RADIATIVE INTERCHANGE BETWEEN CONDUCTING FINS WITH MUTUAL IRRADIATIONS. Max. A. Heaslet and Harvard Lomax. 1961. i, 22 p. diagrs., tab. GPO price 35 cents. (NASA TECHNICAL REPORT R-116)

Analytical and numerical methods are developed that predict the flux of radiant energy from a family of thin, planar, conducting fins. For a symmetrical array of fins, extending out from a common edge, conducting heat internally, and radiating diffusely, a nonlinear integro-differential equation is derived and solved. Specific results are given for parametric variations of conduction, emissivity, fin geometry, and base temperature. The techniques of calculation are studied with possible extensions in mind.

(Initial NASA distribution: 2, Aerodynamics, missiles and space vehicles; 26, Materials, other; 27, Mathematics; 33, Physics, theoretical; 35, Power sources, supplementary; 37, Propulsion system elements; 47, Satellites; 51, Stresses and loads; 52, Structures.)

Copies obtainable from Supt. of Docs., GPO Washington

I. Heaslet, Max. A.
II. Lomax, Harvard
III. NASA TR R-116

NASA

NASA TR R-116
National Aeronautics and Space Administration.
NUMERICAL PREDICTIONS OF RADIATIVE INTERCHANGE BETWEEN CONDUCTING FINS WITH MUTUAL IRRADIATIONS. Max. A. Heaslet and Harvard Lomax. 1961. i, 22 p. diagrs., tab. GPO price 35 cents. (NASA TECHNICAL REPORT R-116)

Analytical and numerical methods are developed that predict the flux of radiant energy from a family of thin, planar, conducting fins. For a symmetrical array of fins, extending out from a common edge, conducting heat internally, and radiating diffusely, a nonlinear integro-differential equation is derived and solved. Specific results are given for parametric variations of conduction, emissivity, fin geometry, and base temperature. The techniques of calculation are studied with possible extensions in mind.

(Initial NASA distribution: 2, Aerodynamics, missiles and space vehicles; 26, Materials, other; 27, Mathematics; 33, Physics, theoretical; 35, Power sources, supplementary; 37, Propulsion system elements; 47, Satellites; 51, Stresses and loads; 52, Structures.)

Copies obtainable from Supt. of Docs., GPO Washington

I. Heaslet, Max. A.
II. Lomax, Harvard
III. NASA TR R-116

NASA